

# Distribution of write error rate of spin-transfer-torque magnetoresistive random access memory caused by a distribution of junction parameters<sup>☆</sup>

Hiroshi Imamura, Hiroko Arai, Rie Matsumoto

*National Institute of Advanced Industrial Science and Technology (AIST), Tsukuba, Ibaraki 305-8568, Japan*

## Abstract

Distribution of write error rate (WER) of spin-transfer-torque magnetoresistive random access memory (STT MRAM) caused by a distribution of resistance area product and anisotropy constant is theoretically studied. Assuming that WER is much smaller than unity, and junction parameters obey a normal distribution, we show that the WER obeys a logarithmic normal distribution. We derive analytical expressions for the probability density function and statistical measures. We find that the coefficient of variation of WER can be reduced by decreasing the pulse width. We also perform numerical simulations based on the Fokker-Planck equation and confirm the validity of the analytical expressions. The results are useful for designing reliable STT MRAMs.

**Keywords:** spin transfer torque, magnetoresistive random access memory, write error rate, probability distribution function, logarithmic normal distribution

## 1. Introduction

Spin-transfer-torque magnetoresistive random access memory (STT MRAM) has been attracting much attention as a key component for future low-power electronics because of its useful characteristics such as high integration density, non-volatility, low-latency, and high-endurance [1–9]. In STT MRAM information is written as stable magnetic states which are separated by energy barrier due to magnetic anisotropy by using the STT switching method [10–12]. Magnetoresistance effect is used to read the information. The magnetic tunnel junction (MTJ) which comprises a MgO insulating barrier sandwiched by Fe-based magnetic electrodes is widely used as a basic element of STT MRAM because of the large magnetoresistance ratio [13–15] as well as of perpendicular magnetic anisotropy [16–18]. The perpendicularly magnetized MgO-based MTJ paved the way for a variety of applications of STT MRAM [19–21]. For all applications reliability is an important quality factor.

Write error rate (WER), i.e. probability of switching failure, is a key metric to characterize the reliability of STT MRAM [4, 22–30]. Magnetization switching by STT is an intrinsically stochastic process because the magnetization dynamics is disturbed by thermal agitation fields. Although much effort has been devoted to the study of WER of single memory cell, little attention has been paid to the statistical properties of an ensemble of memory cells with a distribution of junction parameters such as resistance area product (RA) and anisotropy constant. For developing a reliable STT MRAM it is important to understand the impact of a distribution of junction parameters on a

distribution of WER of an ensemble of memory cells and to find a way to reduce the coefficient of variation (CV), i.e. the ratio of the standard deviation to the expectation value, of WER.

Recently Arai et al. studied the probability distribution of WER of voltage controlled (VC) MRAM [31]. VC MRAM is another type of MRAM which utilizes the voltage controlled magnetic anisotropy effect to switch the magnetization and is in the basic research stage [32–36]. Assuming that the anisotropy constant of memory cells obeys a normal distribution they derived an analytical expression of the probability density function (PDF) of WER and classify the shape of PDF into two classes depending on the mean and standard deviation of the anisotropy constant. Their analysis can be applied to the case of STT MRAM.

In this paper, following Ref. [31], we analyze the distribution of WER of STT MRAM caused by a distribution of RA and anisotropy constant. Assuming that WER is much smaller than unity, and the junction parameters obey a normal distribution, we show that the WER obeys a logarithmic normal distribution. Analytical expressions for the PDF and statistical measures are derived, which show that the CV of WER can be reduced by decreasing the pulse width. The validity of analytical expressions are confirmed by numerical simulations based on the Fokker-Planck (FP) equation.

## 2. Theoretical model

We analyze the STT switching of the magnetization in the free layer (FL) of a circular-shaped MTJ-nanopillar shown in Fig. 1(a). The insulating layer indicated in gray is sandwiched by the two ferromagnetic layers: the FL and the reference layer (RL). The direction of the magnetization in the FL is represented by the unit vector  $\mathbf{m} = (m_x, m_y, m_z)$ . The magnetization

<sup>☆</sup>This work is partly supported by JSPS KAKENHI Grant Numbers JP19H01108, No. JP20K12003.

Email addresses: h-imamura@aist.go.jp (Hiroshi Imamura), arai-h@aist.go.jp (Hiroko Arai)

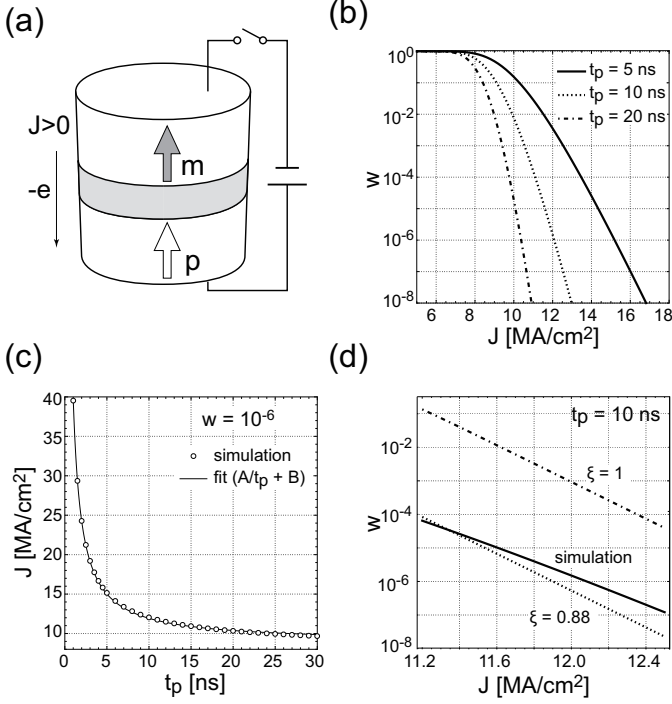


Figure 1: (a) Magnetic tunnel junction nano pillar with circular cylinder shape. The magnetization unit vectors in the free layer (FL) and in the reference layer (RL) are represented by  $\mathbf{m}$  and  $\mathbf{p}$ , respectively. The positive current density,  $J > 0$ , is defined as electrons flowing from the FL to the RL. (b)  $J$  dependence of WER,  $w$ , for pulse width of  $t_p = 5$  ns (solid), 10 ns (dotted), and 20 ns (dot-dashed). (c)  $t_p$  dependence of  $J$  required to achieve  $w = 10^{-6}$ . The open circles indicate the simulation results. The solid curve represents a fit by the function of  $A/t_p + B$ , where  $A$  and  $B$  are fitting parameters. (d)  $J$  dependence of  $w$  for  $t_p = 10$  ns. The solid curve indicates the simulation results. The dotted curve shows Eq. (22) with  $\xi = 0.88$ , where  $\xi$  is a renormalization coefficient of anisotropy constant. The dot-dashed curve shows Eq. (22) with  $\xi = 1$ .

unit vector in the RL is represented by  $\mathbf{p}$  and is fixed to align in the positive  $z$  direction, i.e.  $\mathbf{p} = (0, 0, 1)$ . The  $z$  axis is taken to be the out-of-plane direction and the  $x$  and  $y$  axes are taken to be the in-plane directions. The positive current density,  $J > 0$ , is defined as electrons flowing from the FL to the RL. The size of the nanopillar is assumed to be so small that the magnetization dynamics can be described by the macrospin model.

The dynamics of the magnetization unit vector in the FL are calculated by solving the following Landau-Lifshitz-Gilbert (LLG) equation with STT term,

$$\frac{d\mathbf{m}}{dt} = -\gamma\mathbf{m} \times \mathbf{H}_{\text{eff}} - \gamma\chi\mathbf{m} \times (\mathbf{m} \times \mathbf{p}) + \alpha\mathbf{m} \times \frac{d\mathbf{m}}{dt}, \quad (1)$$

where the first, second, and third terms on the right hand side represent the torque due to the effective field,  $\mathbf{H}_{\text{eff}}$ , STT, and damping torque, respectively. Here  $\gamma$  is the gyromagnetic ratio,  $\chi$  is the coefficient of STT, and  $\alpha$  is the Gilbert damping constant. The effective field comprises the anisotropy field,  $\mathbf{H}_{\text{anis}}$ , and the thermal agitation field,  $\mathbf{H}_{\text{therm}}$ , as

$$\mathbf{H}_{\text{eff}} = \mathbf{H}_{\text{anis}} + \mathbf{H}_{\text{therm}}. \quad (2)$$

The anisotropy field is given by

$$\mathbf{H}_{\text{anis}} = \frac{2Km_z}{\mu_0 M_s} \mathbf{e}_z, \quad (3)$$

where  $K$  is the anisotropy constant,  $\mu_0$  is vacuum permeability, and  $M_s$  is the saturation magnetization,  $\mathbf{e}_z$  is the unit vector in the positive  $z$  direction. The thermal agitation field is determined by the fluctuation-dissipation theorem [37–40] and satisfies the following relations:  $\langle H_{\text{therm}}^i(t) \rangle = 0$  and

$$\langle H_{\text{therm}}^i(t) H_{\text{therm}}^j(t') \rangle = \mu \delta_{i,j} \delta(t - t'), \quad (4)$$

where  $\langle \rangle$  represents the statistical mean, indices  $i, j$  denote the  $x, y$ , and  $z$  components of the thermal agitation field.  $\delta_{i,j}$  represents Kronecker's delta, and  $\delta(t - t')$  represents Dirac's delta function. The coefficient  $\mu$  is given by

$$\mu = \frac{2\alpha k_B T}{\gamma \mu_0 M_s \Lambda}, \quad (5)$$

where  $k_B$  is the Boltzmann constant,  $T$  is temperature, and  $\Lambda$  is the volume of the FL. The coefficient of STT,  $\chi$ , is defined as

$$\chi = \frac{\hbar P J}{2e\mu_0 M_s d}, \quad (6)$$

where  $\hbar$  is Dirac's constant,  $P$  is the spin polarization of the current,  $e$  is the elementary charge,  $d$  is the thickness of the FL [10, 41]. The angle dependence of  $\chi$  is neglected for simplicity. At  $T = 0$  the critical current density over which  $\mathbf{m}$  is switched by STT is determined by competition between the STT and the damping torque and is obtained as [42–44]

$$J_c = \frac{4\alpha e d K}{\hbar P}. \quad (7)$$

Throughout this paper, the following typical parameters are assumed.  $\alpha = 0.05$ ,  $K = 0.11$  MJ/m<sup>3</sup>,  $M_s = 1$  MA/m. The diameter of the MTJ nano-pillar is 40 nm. The thickness of the FL is  $d = 1.1$  nm. The spin polarization of current is  $P = 0.6$ , the RA is  $10 \Omega\mu\text{m}^2$ , and the temperature is  $T = 300$  K. These parameters give the thermal stability factor of  $\Delta_K = 60$  and the critical current density for STT switching of  $J_c = 10$  MA/cm<sup>2</sup>.

### 3. Simulation method

Magnetization switching is an intrinsically stochastic process because of thermal agitation. Effects of thermal agitation on STT induced magnetization switching can be analyzed based on the FP equation. Following Brown [37] we introduce the spherical coordinate defined as  $\mathbf{m} = (\sin \theta \cos \phi, \sin \theta \sin \phi, \cos \theta)$ , where  $\theta$  and  $\phi$  are the polar angle and the azimuthal angle, respectively. The direction of  $\mathbf{m}$  is represented by the point on a unit sphere identified by the angles  $\theta$  and  $\phi$ . The statistical properties of  $\mathbf{m}$  are represented by the PDF,  $F(\theta, \phi)$ . Since the system has a rotational symmetry around  $z$  axis, the statistical properties do not depend on  $\phi$ . Introducing the PDF of  $\theta$  defined as  $W(\theta) = \int_0^{2\pi} F(\theta, \phi) d\phi$ , the FP equation for  $W(\theta)$  is obtained as

$$\frac{\partial W}{\partial t} = a \frac{1}{\sin \theta} \frac{\partial}{\partial \theta} \left[ \sin \theta \left( \frac{\partial \epsilon}{\partial \theta} \right) W + \frac{1}{\beta} \sin \theta \frac{\partial W}{\partial \theta} \right], \quad (8)$$

where  $\beta = \Lambda/(k_B T)$  is the inverse of the thermal energy density, the coefficient  $a$  is given by

$$a = \frac{\alpha \gamma}{(1 + \alpha^2) M_s}, \quad (9)$$

and  $\epsilon$  is the effective energy density defined as

$$\epsilon = K \sin^2 \theta + \frac{\mu_0 M_s^2}{\alpha} \chi \cos \theta. \quad (10)$$

Introducing  $\zeta = \cos \theta$  the FP equation and the effective energy density are expressed as

$$\frac{\partial W}{\partial \tau} = a \frac{\partial}{\partial \zeta} \left\{ (1 - \zeta^2) \left[ \left( \frac{\partial \epsilon}{\partial \zeta} \right) W + \frac{1}{\beta} \left( \frac{\partial W}{\partial \zeta} \right) \right] \right\}, \quad (11)$$

and

$$\epsilon = K (1 - \zeta^2) + \frac{\mu_0 M_s^2}{\alpha} \chi \zeta. \quad (12)$$

Then we introduce the dimensionless time,  $\tau$ , thermal stability factor,  $\Delta_K$ , and the dimensionless parameter characteristic for STT,  $\Delta_J$ , which are respectively defined as

$$\tau = \frac{\alpha \gamma}{1 + \alpha^2} \frac{k_B T}{M_s \Lambda} t, \quad (13)$$

$$\Delta_K = \frac{K \Lambda}{k_B T}, \quad (14)$$

and

$$\Delta_J = -\frac{\mu_0 M_s^2 \chi \Lambda}{\alpha k_B T} \quad (15)$$

to obtain the dimensionless form of the FP equation,

$$\begin{aligned} \frac{\partial W}{\partial \tau} = & -2\Delta_K W + 2\Delta_J \zeta W + 6\Delta_K \zeta^2 W \\ & - \Delta_J (1 - \zeta^2) \frac{\partial W}{\partial \zeta} - 2\Delta_K \zeta (1 - \zeta^2) \frac{\partial W}{\partial \zeta} \\ & + \frac{\partial}{\partial \zeta} \left[ (1 - \zeta^2) \left( \frac{\partial W}{\partial \zeta} \right) \right]. \end{aligned} \quad (16)$$

Equation (16) is solved by using the Legendre polynomial expansion,

$$W(\tau, \zeta) = \sum_{n=0}^{\infty} c_n(\tau) P_n(\zeta), \quad (17)$$

where  $P_n(\zeta)$  is the  $n$ th Legendre function. Substituting Eq. (17) into Eq. (16) we obtain the following equation of motion for the coefficient of the Legendre polynomial,

$$\begin{aligned} \frac{\partial c_n(\tau)}{\partial \tau} = & 2\Delta_K \frac{(n-1)n(n+1)}{(2n-3)(2n-1)} c_{n-2}(\tau) \\ & + \Delta_J \frac{n(n+1)}{2n-1} c_{n-1}(\tau) \\ & + n(n+1) \left[ \frac{2\Delta_K}{(2n-1)(2n+3)} - 1 \right] c_n(\tau) \\ & - \Delta_J \frac{n(n+1)}{2n+3} c_{n+1}(\tau) \\ & - 2\Delta_K \frac{n(n+1)(n+2)}{(2n+3)(2n+5)} c_{n+2}(\tau). \end{aligned} \quad (18)$$

The initial distribution is prepared by relaxing  $W(\zeta)$  from the delta function at  $\zeta = 1$  for 5 ns without applying current. Then switching dynamics of  $W(\zeta)$  are calculated under application of current during the pulse width,  $t_p$ . After the pulse the magnetization is relaxed without applying current for 5 ns. Then the WER is evaluated by integrating  $W(\zeta)$  from 0 to 1. The basis set with 100 Legendre functions has already been enough for a converged result. The validity of the preparation procedure of the initial distribution is discussed in [Appendix A](#).

## 4. Results

### 4.1. WER without distribution of junction parameters

Before discussing the impact of a distribution of junction parameters such as RA and anisotropy constant on a distribution of WER, we briefly show basic properties of WER of STT switching without a distribution of junction parameters. Figure 1(b) shows the typical examples of the logarithmic plot of the WER,  $w$ , as a function of current density. Here and hereafter the symbol  $w$  stands for the WER. The solid, dotted, and dot-dashed curves indicate the results for  $t_p = 5, 10$ , and 20 ns, respectively. The WER suddenly drops just before the critical current density of  $J_c = 10$  MA/cm<sup>2</sup> because the magnetization can switch owing to thermal agitation even below  $J_c$ . From a practical application point of view we are interested in the low WER regime, e.g.  $w \sim 10^{-6}$ . As shown in Fig. 1(b) the WER exponentially decreases with increase of  $J$  in the low WER regime, which qualitatively agrees with the analytical expressions given in Refs. [22, 28]. Assuming that thermally distributed initial magnetization states determine the distribution of switching time for  $J \gg J_c$ , the WER is expressed as [28]

$$w = 1 - \exp \left\{ -4\Delta_K \exp \left[ -\left( \frac{J}{J_c} - 1 \right) \frac{2t_p}{t_D} \right] \right\}, \quad (19)$$

where  $t_D$  is a characteristic time scale for switching dynamics defined as

$$t_D = \frac{(1 + \alpha^2) M_s}{2\alpha \gamma K}. \quad (20)$$

In the case of  $w \ll 1$  Eq. (19) is approximated as

$$w = 4\Delta_K \exp \left[ -\left( \frac{J}{J_c} - 1 \right) \frac{2t_p}{t_D} \right]. \quad (21)$$

Although Eq. (21) is valid for  $J \gg J_c$  where thermal agitation field during the precession is neglected, numerical simulation results shown in Fig. 1(b) implies that the current dependence of the WER takes the similar form as Eq. (21) even in the region  $J \sim J_c$  as long as  $w \ll 1$ . In Ref. [28], they analyzed the experimental data by treating  $\Delta_K$  and  $t_D$  as fitting parameters. Here we made a crude approximation that the effect of thermal agitation field can be taken into account by renormalizing the anisotropy constant. Introducing the renormalization coefficient  $\xi$ , the parameters  $K$ ,  $J_c$ , and  $t_D$  are renormalized as  $\xi K$ ,  $\xi J_c$ , and  $t_D/\xi$ , respectively. The coefficient  $\xi$  is determined by fitting the  $t_p$  dependence of  $J$  required to achieve  $w = 10^{-6}$ . As pointed out

in Refs. [28, 45, 46] the current density required for a certain switching probability is inversely proportional to  $t_p$  when STT gives a dominant contribution to the switching dynamics. In Fig. 1(c) the simulation results of the  $t_p$  dependence of  $J$  for  $w = 10^{-6}$  is shown by the open circles. The simulation results are well fitted by the function  $J = A/t_p + B$  with  $A = 3.1 \times 10^{11}$  C/m<sup>2</sup> and  $B = 8.8 \times 10^{10}$  A/m<sup>2</sup> shown by the solid curve. Since the fitting parameter  $B$  corresponds to the renormalized critical current density, the renormalization coefficients are determined as  $\xi = B/J_c = 0.88$ . In terms of the renormalized parameters, the WER is expressed as

$$w = 4\xi\Delta_K \exp\left[-\left(\frac{J}{\xi J_c} - 1\right)\frac{2\xi t_p}{t_D}\right]. \quad (22)$$

Figure 1(d) shows the  $J$  dependence of  $w$  in the low WER regime for  $t_p = 10$  ns. The simulation results obtained by numerically solving Eq. (16) is plotted by the solid curve. Equation (22) with  $\xi = 0.88$  and  $\xi = 1$  are plotted by the dotted and dot-dashed curves, respectively. The simulation results are well reproduced by Eq. (22) with  $\xi = 0.88$ .

#### 4.2. WER distribution due to RA distribution

In this subsection we analyze impact of a distribution of RA on a distribution of WER. Let  $r$  denote the value of RA and is assumed to obey a normal distribution with mean of  $r_0$  and standard deviation of  $\sigma$ ,

$$f(r) = \frac{1}{\sqrt{2\pi}\sigma} \exp\left\{-\frac{(r-r_0)^2}{2\sigma^2}\right\}. \quad (23)$$

The PDF of  $w$ , which is denoted by  $g(w)$ , is obtained by using the change of the variable technique [31, 47] as

$$g(w) = f(r) \left| \frac{dr}{dw} \right|. \quad (24)$$

We first derive the analytical expression of  $g(w)$  using Eqs. (21), (23), and (24). Then we show that  $g(w)$  can be expressed as a logarithmic normal distribution if  $\log(w)$  can be approximated as a linear function of  $\delta r$ , where  $\delta r = r - r_0$ .

##### 4.2.1. Derivation of $g(w)$ based on the change of variable technique

Let  $V$  denote the applied bias voltage defined as  $J = V/r$ . The logarithm of Eq. (22) is expressed as

$$\log(w) = -\frac{b}{r} + c, \quad (25)$$

where

$$b = \frac{\hbar \gamma V P t_p}{(1 + \alpha^2) M_s d e} \quad (26)$$

and

$$c = \log(4\xi\Delta_K) + \frac{2\xi t_p}{\tau_D}. \quad (27)$$

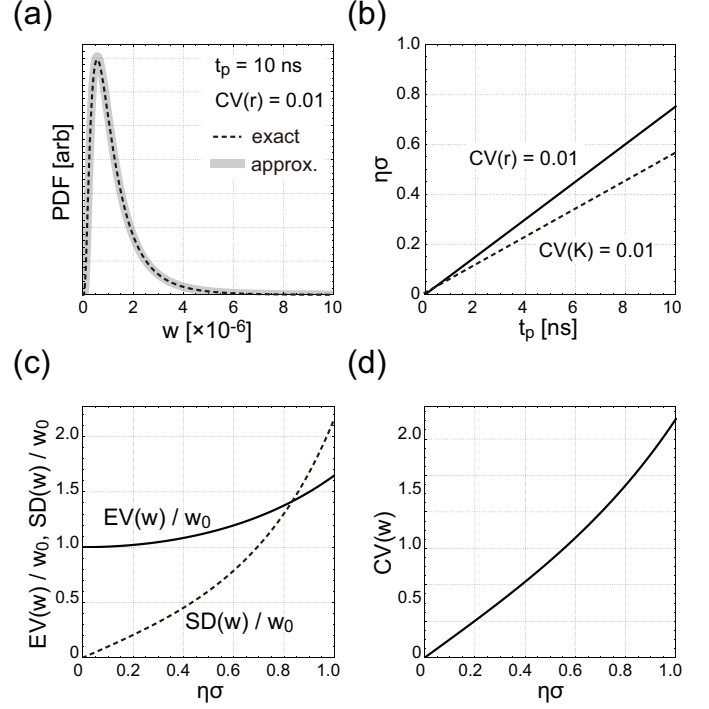


Figure 2: (a) Probability density function (PDF) of write error rate (WER),  $w$ , for pulse width of  $t_p = 10$  ns. The resistance area product,  $r$ , is assumed to obey a normal distribution with coefficient of variation (CV) of 0.01. (b)  $t_p$  dependence of  $\eta\sigma$  which represents the standard deviation of  $\log(w)$ . Solid line represents the result for the case  $r$  obeys a normal distribution with  $CV(r) = 0.01$ . Dotted line represents the result for the case that the anisotropy constant,  $K$ , obeys a normal distribution with  $CV(K) = 0.01$ . (c) Normalized expectation value,  $EV(w)/w_0$ , (solid) and normalized standard deviation,  $SD(w)/w_0$ , (dotted) as functions of  $\eta\sigma$ .  $w_0$  is the WER without distribution of junction parameters. (d)  $CV(w)$  as a function of  $\eta\sigma$ .

Then the derivative of  $r$  in terms of  $w$  is obtained as

$$\frac{dr}{dw} = \frac{b}{w[c - \log(w)]^2}. \quad (28)$$

Substituting Eqs. (23) and (28) into Eq. (24) the PDF of  $w$  is obtained as

$$g(w) = \frac{q(w)^2}{\sqrt{2\pi} b \sigma w} \exp\left\{-\frac{[q(w) - q(w_0)]^2}{2\sigma^2}\right\}, \quad (29)$$

where the function  $q(w)$  is defined as

$$q(w) = \frac{b}{c - \log(w)}. \quad (30)$$

In Fig. 2(a) we plot Eq. (29) for  $t_p = 10$  ns by the dotted curve. The CV of  $r$  is assumed to be  $CV(r) = 0.01$ .  $g(w)$  has a large skewness although  $f(r)$  is assumed to be a normal distribution. In Sec. 4.2.2, we show that  $g(w)$  can be approximated as the logarithmic normal distribution shown by the thick gray curve in Fig. 2(a).



#### 4.2.2. Derivation of an approximate expression of $g(w)$ using the linear approximation of $\log(w)$

Introducing

$$\eta = \frac{\hbar \gamma V P t_p}{(1 + \alpha^2) M_s d e r_0^2}, \quad (31)$$

and take the first order of  $\delta r$ , Eq. (25) can be approximated as

$$\log(w) = \log(w_0) + \eta \delta r. \quad (32)$$

As shown in Fig. 2(b)  $\eta\sigma$  is a linear increasing function of  $t_p$  and is less than 0.8 for  $t_p \leq 10$  ns. Then  $\delta r$  is expressed as

$$\delta r = \frac{1}{\eta} \log\left(\frac{w}{w_0}\right), \quad (33)$$

of which PDF is given by

$$f(\delta r) = \frac{1}{\sqrt{2\pi}\sigma} \exp\left(-\frac{\delta r^2}{2\sigma^2}\right). \quad (34)$$

Substituting Eqs. (33) and (34) into Eq. (24),  $g(w)$  is obtained as

$$g(w) = \frac{1}{\sqrt{2\pi}\eta\sigma w} \exp\left\{-\frac{[\log(w) - \log(w_0)]^2}{2\eta^2\sigma^2}\right\}, \quad (35)$$

which is a logarithmic normal distribution of  $w$ . Eq. (35) tells us that  $\log(w)$  obeys a normal distribution with mean of  $\log(w_0)$  and standard deviation of  $\eta\sigma$ . Equation (35) for  $t_p = 10$  ns is plotted by the thick gray curve in Fig. 2(a), which agrees well with the exact result of Eq. (29).

The expectation value of  $w$  is given by

$$EV(w) = \exp\left[\log(w_0) + \frac{\eta^2\sigma^2}{2}\right], \quad (36)$$

which is larger than  $w_0$  and increases with increase of  $\eta\sigma$ . The standard deviation is given by

$$SD(w) = EV(w) \sqrt{\exp(\eta^2\sigma^2) - 1}, \quad (37)$$

which increases more rapidly with increase of  $\eta\sigma$  compared with  $EV(w)$  as shown in Fig. 2(c) by the dotted curve. The coefficient of variation, which is a relative measure of dispersion and is defined as the ratio of  $SD(w)$  to  $EV(w)$ , is given by

$$CV(w) = \sqrt{\exp(\eta^2\sigma^2) - 1}, \quad (38)$$

which is an increasing function of  $\eta\sigma$  as shown in Fig. 2(d). Since  $\eta\sigma$  is a linear increasing function of  $t_p$ ,  $CV(w)$  can be reduced by decreasing  $t_p$ .

#### 4.3. WER distribution due to a distribution of anisotropy constant

In this subsection we study a distribution of WER caused by a distribution of anisotropy constant,  $K$ . We assume that  $K$  obeys a normal distribution with mean of  $K_0$  and standard deviation

of  $\sigma$ . The probability distribution function of  $\delta K = K - K_0$  is given by

$$f(\delta K) = \frac{1}{\sqrt{2\pi}\sigma} \exp\left(-\frac{\delta K^2}{2\sigma^2}\right). \quad (39)$$

Similar to Eq. (32) we approximate  $\log(w)$  up to the first order of  $\delta K$  as

$$\log(w) = \log(w_0) + \eta \delta K, \quad (40)$$

where  $w_0$  is the WER at  $K_0$  and the coefficient  $\eta$  is now defined as

$$\eta = \frac{1}{K_0} \left(1 + \frac{2\xi t_p}{t_D^0}\right). \quad (41)$$

Here  $t_D^0 = (1 + \alpha^2)M_s/(2\alpha\gamma K_0)$ . The  $t_p$  dependence of  $\eta\sigma$  for  $CV(K) = 0.01$  is shown by the dotted line in Fig. 2(b).  $\eta\sigma$  is a linear increasing function of  $t_p$  and is less than 0.6 for  $t_p \leq 10$  ns. The PDF of  $w$  is given by Eq. (35) with  $\eta$  defined by Eq. (41). The expectation value, standard deviation, and coefficient of variation are also given by the same equations as Eqs. (36), (37), and (38), respectively, with  $\eta$  defined by Eq. (41). Similar to the case with a distribution of  $r$ , the CV can be reduced by decreasing  $t_p$ .

#### 4.4. Comparison with numerical simulations

In the preceding subsections, we derive the analytical expressions for the PDF and statistical measures of WER and showed that the CV can be reduced by decreasing  $t_p$  both for the case with a distribution of RA and anisotropy constant. In this subsection we perform numerical simulations based on the FP equation to confirm the validity of the analytical results.

Figure 3(a) shows the  $t_p$  dependence of  $EV(w)/w_0$  and  $SD(w)/w_0$  for the case that RA obeys a normal distribution with  $CV(r) = 0.01$ . The simulation results are represented by the solid curves, and the analytical results are plotted by the dotted curves. For both  $EV(w)/w_0$  and  $SD(w)/w_0$  the curves representing simulation results and analytical results intersect each other around  $t_p = 6$  ns. For  $t_p \gtrless 6$  ns, analytical results overestimate  $EV(w)/w_0$  and  $SD(w)/w_0$ , and the difference between the simulation and analytical results increases with increase of  $t_p$ . The  $t_p$  dependence of  $CV(w)$  is shown in Fig. 3(b). Both the simulation result and the analytical result are increasing function of  $t_p$ , which confirms the validity of the analytical prediction that CV can be reduced by decreasing  $t_p$ . Similar to  $EV(w)$  and  $SD(w)$ , the analytical results under estimate (over estimate) the  $CV(w)$  for  $t_p \gtrless 6$  ns ( $t_p \gtrless 6$  ns).

The same plots for the case that  $K$  obeys a normal distribution with  $CV(K) = 0.01$  are shown in Figs. 3(c) and 3(d). The analytical results overestimate  $EV(w)$ ,  $SD(w)$ , and  $CV(w)$  in the entire range of the plot, and the difference between the simulation results and analytical results increases with increase of  $t_p$ . Similar to the results in Fig. 3(b), the simulation results of  $CV(w)$  is an increasing function of  $t_p$ . Therefore we conclude that  $CV(w)$  can be reduced by decreasing  $t_p$  both for the case with a distribution of RA and anisotropy constant. Simulation with  $CV(K) = 0.01$  shows that  $CV(w)$  is as large as 0.49 for  $t_p = 10$  ns and can be reduced 0.065 by decreasing  $t_p$  to 1 ns.

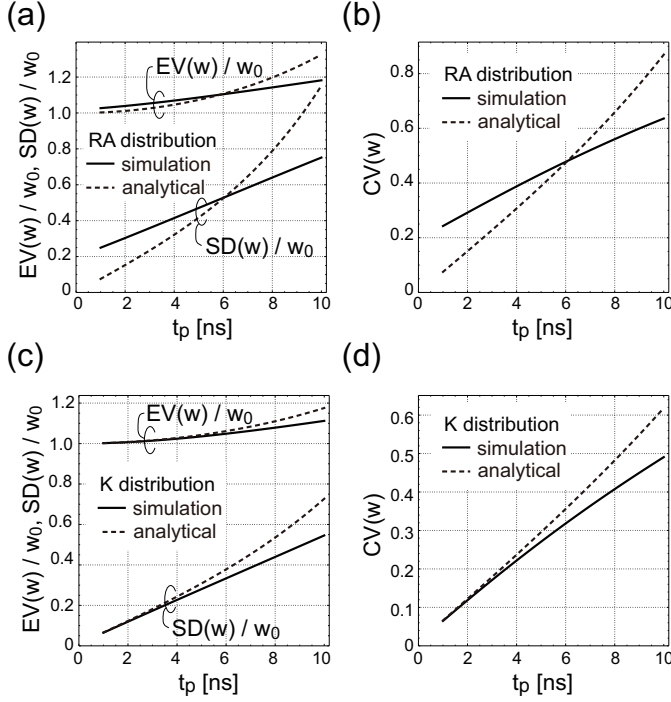


Figure 3: (a) Pulse width,  $t_p$ , dependence of normalized expectation value,  $EV(w)/w_0$ , and normalized standard deviation,  $SD(w)/w_0$ , for the case that resistance area product (RA),  $r$ , obeys a normal distribution with the coefficient of variation (CV) of  $CV(r) = 0.01$ .  $w$  and  $w_0$  represent the write error rate (WER) with and without a distribution of junction parameters, respectively. (b)  $t_p$  dependence of the coefficient of variation of  $w$ ,  $CV(w)$ , for  $CV(r) = 0.01$ . (c) The same plot as (a) for the case that anisotropy constant,  $K$ , obeys a normal distribution with  $CV(K) = 0.01$ . (d) The same plot as (b) for  $CV(K) = 0.01$ . In all panels the solid and dotted curves represent the simulation and analytical results, respectively.

## 5. Summary

In summary, we theoretically study a distribution of WER of STT MRAM caused by a distribution of junction parameters, i.e. RA and anisotropy constant. Assuming that WER is much smaller than unity, and the junction parameters obey a normal distribution, we derive analytical expressions of the probability density function and statistical measures. We find that the WER obeys a logarithmic normal distribution and the CV of WER can be reduced by decreasing pulse width. The validity of the analytical results is confirmed by numerical simulations. The results provide important insights into statistical properties of STT switching and are useful for designing reliable STT MRAM.

## Appendix A. Validity of the preparation procedure of the initial distribution

In this section we discuss the validity of the preparation procedure of the initial distribution of  $\zeta$ . As mentioned in the last paragraph of Sec. 3, the initial distribution is prepared by relaxing  $W(\zeta)$  from the delta function at  $\zeta = 1$  for 5 ns without applying current. In terms of the Legendre polynomials, the

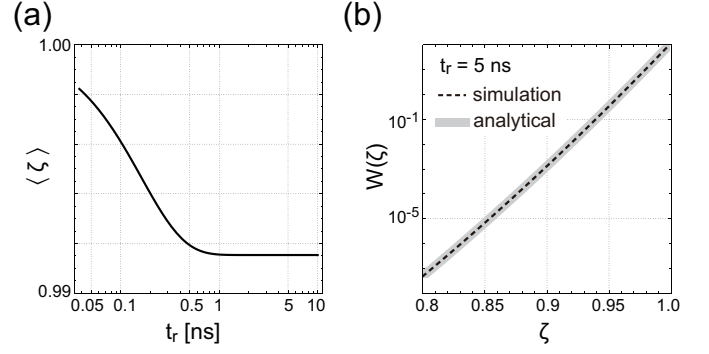


Figure A.1: (a) Relaxation time,  $t_r$ , dependence of the expectation value of  $\zeta$ ,  $\langle \zeta \rangle$ . (b) Initial distribution of  $\zeta$ . The dotted black curve represents the initial distribution obtained by numerically solving the FP equation. The thick gray curve represents the distribution given by Eq. (A.3).

delta function at  $\zeta = 1$  is expressed as

$$\delta(1 - \zeta) = \sum_{n=0}^{\infty} \frac{2n+1}{2} P_n(\zeta). \quad (\text{A.1})$$

In numerical calculations 100 Legendre functions are used to represent the delta function.

Figure A.1(a) show the relaxation time,  $t_r$ , dependence of the expectation value of  $\zeta$ , which is obtained as

$$\langle \zeta \rangle = \int_{-1}^1 \zeta W(\zeta, t_r) d\zeta = \frac{2}{3} c_1(t_r). \quad (\text{A.2})$$

The expectation value of  $\zeta$  decreases with increase of  $t_r$  and converges to the value of 0.9915 about  $t_r = 1$  ns.

In the absence of current, the system has two equivalent energy minima at  $\zeta = \pm 1$  and the thermal equilibrium value of  $\zeta$  is 0. However, since the thermal stability constant is assumed to be as large as 60 it takes more than tens of years to reach the thermal equilibrium. On time scale of nano-seconds the distribution of  $\zeta$  is represented by the Boltzmann distribution localized on the upper hemisphere ( $\zeta > 0$ ), which is defined as

$$W(\zeta) = \frac{2\sqrt{\Delta_K}}{\sqrt{\pi} \text{Erfi}(\sqrt{\Delta_K})} \exp[\Delta_K \zeta^2], \quad (\text{A.3})$$

where  $\text{Erfi}(\zeta)$  denotes the imaginary error function of  $\zeta$ . The converged value of  $\langle \zeta \rangle = 0.9915$  is the same as the expectation value calculated using Eq. (A.3).

In Fig. A.1(b), the distribution function,  $W(\zeta)$ , obtained by numerically solving the FP equation is plotted by the dotted black curve. The relaxation time is assumed to be  $t_r = 5$  ns. The distribution function given by Eq. (A.3) is also plotted by the thick gray curve. The good agreement between these two curves guarantees the validity of our preparation procedure of the initial distribution.

## Appendix A. Validity of the preparation procedure of the initial distribution

In this section we discuss the validity of the preparation procedure of the initial distribution of  $\zeta$ . As mentioned in the last

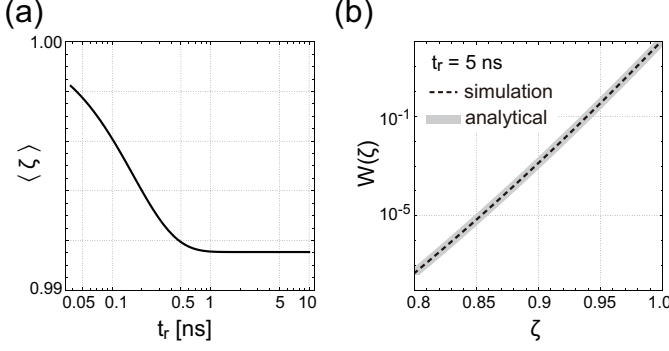


Figure A.1: (a) Relaxation time,  $t_r$ , dependence of the expectation value of  $\zeta$ ,  $\langle\zeta\rangle$ . (b) Initial distribution of  $\zeta$ . The dotted black curve represents the initial distribution obtained by numerically solving the FP equation. The thick gray curve represents the distribution given by Eq. (A.3).

paragraph of Sec. 3, the initial distribution is prepared by relaxing  $W(\zeta)$  from the delta function at  $\zeta = 1$  for 5 ns without applying current. In terms of the Legendre polynomials, the delta function at  $\zeta = 1$  is expressed as

$$\delta(1 - \zeta) = \sum_{n=0}^{\infty} \frac{2n+1}{2} P_n(\zeta). \quad (\text{A.1})$$

In numerical calculations 100 Legendre functions are used to represent the delta function.

Figure A.1(a) show the relaxation time,  $t_r$ , dependence of the expectation value of  $\zeta$ , which is obtained as

$$\langle\zeta\rangle = \int_{-1}^1 \zeta W(\zeta, t_r) d\zeta = \frac{2}{3} c_1(t_r). \quad (\text{A.2})$$

The expectation value of  $\zeta$  decreases with increase of  $t_r$  and converges to the value of 0.9915 about  $t_r = 1$  ns.

In the absence of current, the system has two equivalent energy minima at  $\zeta = \pm 1$  and the thermal equilibrium value of  $\zeta$  is 0. However, since the thermal stability constant is assumed to be as large as 60 it takes more than tens of years to reach the thermal equilibrium. On time scale of nano-seconds the distribution of  $\zeta$  is represented by the Boltzmann distribution localized on the upper hemisphere ( $\zeta > 0$ ), which is defined as

$$W(\zeta) = \frac{2\sqrt{\Delta_K}}{\sqrt{\pi} \text{Erfi}(\sqrt{\Delta_K})} \exp[\Delta_K \zeta^2], \quad (\text{A.3})$$

where  $\text{Erfi}(\zeta)$  denotes the imaginary error function of  $\zeta$ . The converged value of  $\langle\zeta\rangle = 0.9915$  is the same as the expectation value calculated using Eq. (A.3).

In Fig. A.1(b), the distribution function,  $W(\zeta)$ , obtained by numerically solving the FP equation is plotted by the dotted black curve. The relaxation time is assumed to be  $t_r = 5$  ns. The distribution function given by Eq. (A.3) is also plotted by the thick gray curve. The good agreement between these two curves guarantees the validity of our preparation procedure of the initial distribution.

## References

- [1] S. Yuasa, A. Fukushima, K. Yakushiji, T. Nozaki, M. Konoto, H. Maehara, H. Kubota, T. Taniguchi, H. Arai, H. Imamura, K. Ando, Y. Shiota, F. Bonell, Y. Suzuki, N. Shimomura, E. Kitagawa, J. Ito, S. Fujita, K. Abe, K. Nomura, H. Noguchi, H. Yoda, Future prospects of MRAM technologies, in: 2013 IEEE International Electron Devices Meeting, IEEE, 2013, pp. 3.1.1–3.1.4. doi:10.1109/IEDM.2013.6724549. URL <http://ieeexplore.ieee.org/document/6724549/>
- [2] K. Ando, S. Fujita, J. Ito, S. Yuasa, Y. Suzuki, Y. Nakatani, T. Miyazaki, H. Yoda, Spin-transfer torque magnetoresistive random-access memory technologies for normally off computing (invited), Journal of Applied Physics 115 (2014) 172607. doi:10.1063/1.4869828. URL <http://aip.scitation.org/doi/10.1063/1.4869828>
- [3] A. D. Kent, D. C. Worledge, A new spin on magnetic memories, Nature Nanotechnology 10 (2015) 187–191. doi:10.1038/nnano.2015.24. URL <http://www.nature.com/articles/nnano.2015.24>
- [4] D. Apalkov, B. Dieny, J. M. Slaughter, Magnetoresistive Random Access Memory, Proceedings of the IEEE 104 (2016) 1796–1830. doi:10.1109/JPROC.2016.2590142. URL <https://ieeexplore.ieee.org/document/7555318/>
- [5] R. Sbiaa, S. N. Piramanayagam, Recent Developments in Spin Transfer Torque MRAM, physica status solidi (RRL) - Rapid Research Letters 11 (2017) 1700163. doi:10.1002/pssr.201700163. URL <https://onlinelibrary.wiley.com/doi/10.1002/pssr.201700163>
- [6] H. Cai, W. Kang, Y. Wang, L. Naviner, J. Yang, W. Zhao, High Performance MRAM with Spin-Transfer-Torque and Voltage-Controlled Magnetic Anisotropy Effects, Applied Sciences 7 (2017) 929. doi:10.3390/app7090929. URL <http://www.mdpi.com/2076-3417/7/9/929>
- [7] E. Garzón, M. Lanuzza, R. Taco, S. Strangio, Ultralow Voltage FinFET-Versus TFET-Based STT-MRAM Cells for IoT Applications, Electronics 10 (2021) 1756. doi:10.3390/electronics10151756. URL <https://www.mdpi.com/2079-9292/10/15/1756>
- [8] T. Na, S. H. Kang, S.-O. Jung, STT-MRAM Sensing: A Review, IEEE Transactions on Circuits and Systems II: Express Briefs 68 (2021) 12–18. doi:10.1109/TCSII.2020.3040425. URL <https://ieeexplore.ieee.org/document/9270597/>
- [9] D. C. Worledge, Spin-Transfer-Torque MRAM: the Next Revolution in Memory, in: 2022 IEEE International Memory Workshop (IMW), IEEE, 2022, pp. 1–4. doi:10.1109/IMW52921.2022.9779288. URL <https://ieeexplore.ieee.org/document/9779288/>
- [10] J. Slonczewski, Current-driven excitation of magnetic multilayers, Journal of Magnetism and Magnetic Materials 159 (1996) L1–L7. doi:10.1016/0304-8853(96)00062-5. URL <https://linkinghub.elsevier.com/retrieve/pii/S0304885396000625>
- [11] L. Berger, Emission of spin waves by a magnetic multilayer traversed by a current, Physical Review B 54 (1996) 9353–9358. doi:10.1103/PhysRevB.54.9353. URL <https://link.aps.org/doi/10.1103/PhysRevB.54.9353>
- [12] J. Z. Sun, Spin-transfer torque switched magnetic tunnel junction for memory technologies, Journal of Magnetism and Magnetic Materials 559 (2022) 169479. doi:10.1016/j.jmmm.2022.169479. URL <https://linkinghub.elsevier.com/retrieve/pii/S0304885322004085>
- [13] S. S. P. Parkin, C. Kaiser, A. Panchula, P. M. Rice, B. Hughes, M. Samant, S.-H. Yang, Giant tunnelling magnetoresistance at room temperature with MgO (100) tunnel barriers, Nature Materials 3 (2004) 862–867. doi:10.1038/nmat1256. URL <https://www.nature.com/articles/nmat1256>
- [14] S. Yuasa, T. Nagahama, A. Fukushima, Y. Suzuki, K. Ando, Giant room-temperature magnetoresistance in single-crystal Fe/MgO/Fe magnetic tunnel junctions, Nature Materials 3 (2004) 868–871. doi:10.1038/nmat1257. URL <https://www.nature.com/articles/nmat1257>
- [15] S. Ikeda, J. Hayakawa, Y. Ashizawa, Y. M. Lee, K. Miura, H. Hasegawa, M. Tsunoda, F. Matsukura, H. Ohno, Tunnel magnetoresistance of 604% at 300K by suppression of Ta diffusion in CoFeB/MgO/CoFeB pseudo-spin-valves annealed at high temperature, Applied Physics Letters 93

- (2008) 082508. doi:10.1063/1.2976435.  
URL <http://aip.scitation.org/doi/10.1063/1.2976435>
- [16] M. Nakayama, T. Kai, N. Shimomura, M. Amano, E. Kitagawa, T. Nagase, M. Yoshikawa, T. Kishi, S. Ikegawa, H. Yoda, Spin transfer switching in TbCoFe/CoFeB/MgO/CoFeB/TbCoFe magnetic tunnel junctions with perpendicular magnetic anisotropy, *Journal of Applied Physics* 103 (2008) 07A710. doi:10.1063/1.2838335.  
URL <http://aip.scitation.org/doi/10.1063/1.2838335>
- [17] S. Ikeda, K. Miura, H. Yamamoto, K. Mizunuma, H. D. Gan, M. Endo, S. Kanai, J. Hayakawa, F. Matsukura, H. Ohno, A perpendicular-anisotropy CoFeB–MgO magnetic tunnel junction, *Nature Materials* 9 (2010) 721–724. doi:10.1038/nmat2804.  
URL <https://www.nature.com/articles/nmat2804>
- [18] H. Meng, R. Sbiaa, S. Y. H. Lua, C. C. Wang, M. A. K. Akhtar, S. K. Wong, P. Luo, C. J. P. Carlberg, K. S. A. Ang, Low current density induced spin-transfer torque switching in CoFeB–MgO magnetic tunnel junctions with perpendicular anisotropy, *Journal of Physics D: Applied Physics* 44 (2011) 405001. doi:10.1088/0022-3727/44/40/405001.  
URL <https://iopscience.iop.org/article/10.1088/0022-3727/44/40/405001>
- [19] V. B. Naik, K. Lee, K. Yamane, R. Chao, J. Kwon, N. Thiagarajah, N. L. Chung, S. H. Jang, B. Behin-Aein, J. H. Lim, T. Y. Lee, W. P. Neo, H. Dixit, S. K. L. C. Goh, T. Ling, J. Hwang, D. Zeng, J. W. Ting, E. H. Toh, L. Zhang, R. Low, N. Balasankaran, L. Y. Zhang, K. W. Gan, L. Y. Hau, J. Mueller, B. Pfefferling, O. Kallensee, S. L. Tan, C. S. Seet, Y. S. You, S. T. Woo, E. Quek, S. Y. Siah, J. Pellerin, Manufacturable 22nm FD-SOI Embedded MRAM Technology for Industrial-grade MCU and IOT Applications, in: 2019 IEEE International Electron Devices Meeting (IEDM), IEEE, 2019, pp. 2.3.1–2.3.4. doi:10.1109/IEDM19573.2019.8993454.  
URL <https://ieeexplore.ieee.org/document/8993454/>
- [20] W. Gallagher, E. Chien, T.-W. Chiang, J.-C. Huang, M.-C. Shih, C. Wang, C.-H. Weng, S. Chen, C. Bair, G. Lee, Y.-C. Shih, C.-F. Lee, P.-H. Lee, R. Wang, K.-H. Shen, J. J. Wu, W. Wang, H. Chuang, 22nm STT-MRAM for Reflow and Automotive Uses with High Yield, Reliability, and Magnetic Immunity and with Performance and Shielding Options, in: 2019 IEEE International Electron Devices Meeting (IEDM), IEEE, 2019, pp. 2.7.1–2.7.4. doi:10.1109/IEDM19573.2019.8993469.  
URL <https://ieeexplore.ieee.org/document/8993469/>
- [21] S. Aggarwal, H. Almasi, M. DeHerrera, B. Hughes, S. Ikegawa, J. Janesky, H. K. Lee, H. Lu, F. B. Mancoff, K. Nagel, G. Shimon, J. J. Sun, T. Andre, S. M. Alam, Demonstration of a Reliable 1 Gb Standalone Spin-Transfer Torque MRAM For Industrial Applications, in: 2019 IEEE International Electron Devices Meeting (IEDM), IEEE, 2019, pp. 2.1.1–2.1.4. doi:10.1109/IEDM19573.2019.8993516.  
URL <https://ieeexplore.ieee.org/document/8993516/>
- [22] J. He, J. Z. Sun, S. Zhang, Switching speed distribution of spin-torque-induced magnetic reversal, *Journal of Applied Physics* 101 (2007) 09A501. doi:10.1063/1.2668365.  
URL <http://aip.scitation.org/doi/10.1063/1.2668365>
- [23] D. C. Worledge, G. Hu, P. L. Trouilloud, D. W. Abraham, S. Brown, M. C. Gaidis, J. Nowak, E. J. O'Sullivan, R. P. Robertazzi, J. Z. Sun, W. J. Gallagher, Switching distributions and write reliability of perpendicular spin torque MRAM, in: 2010 International Electron Devices Meeting, IEEE, 2010, pp. 12.5.1–12.5.4. doi:10.1109/IEDM.2010.5703349.  
URL <http://ieeexplore.ieee.org/document/5703349/>
- [24] T. Min, Q. Chen, R. Beach, G. Jan, C. Horng, W. Kula, T. Torng, R. Tong, T. Zhong, D. Tang, P. Wang, M.-m. Chen, J. Z. Sun, J. K. DeBrosse, D. C. Worledge, T. M. Maffitt, W. J. Gallagher, A Study of Write Margin of Spin Torque Transfer Magnetic Random Access Memory Technology, *IEEE Transactions on Magnetism* 46 (2010) 2322–2327. doi:10.1109/TMAG.2010.2043069.  
URL <http://ieeexplore.ieee.org/document/5467625/>
- [25] J. J. Nowak, R. P. Robertazzi, J. Z. Sun, G. Hu, D. W. Abraham, P. L. Trouilloud, S. Brown, M. C. Gaidis, E. J. O'Sullivan, W. J. Gallagher, D. C. Worledge, Demonstration of ultralow bit error rates for spin-torque magnetic random-access memory with perpendicular magnetic anisotropy, *IEEE Magnetism Letters* 2 (2011) 3000204–3000204. doi:10.1109/LMAG.2011.2155625.  
URL <https://ieeexplore.ieee.org/document/5875962/>
- [26] H. Sun, C. Liu, T. Min, N. Zheng, T. Zhang, Architectural Exploration to Enable Sufficient MTJ Device Write Margin for STT-RAM Based Cache, *IEEE Transactions on Magnetism* 48 (2012) 2346–2351. doi:10.1109/TMAG.2012.2193589.  
URL <https://ieeexplore.ieee.org/document/6179331/>
- [27] W. H. Butler, T. Mewes, C. K. A. Mewes, P. B. Visscher, W. H. Rippard, S. E. Russek, R. Heindl, Switching Distributions for Perpendicular Spin-Torque Devices Within the Macrospin Approximation, *IEEE Transactions on Magnetism* 48 (2012) 4684–4700. doi:10.1109/TMAG.2012.2209122.  
URL <http://ieeexplore.ieee.org/document/6242414/>
- [28] H. Liu, D. Bedau, J. Sun, S. Mangin, E. Fullerton, J. Katine, A. Kent, Dynamics of spin torque switching in all-perpendicular spin valve nanopillars, *Journal of Magnetism and Magnetic Materials* 358–359 (2014) 233–258. doi:10.1016/j.jmmm.2014.01.061.  
URL <https://linkinghub.elsevier.com/retrieve/pii/S0304885314000729>
- [29] R. Matsumoto, H. Arai, S. Yuasa, H. Imamura, Theoretical analysis of thermally activated spin-transfer-torque switching in a conically magnetized nanomagnet, *Physical Review B* 92 (2015) 140409(R). doi:10.1103/PhysRevB.92.140409.  
URL <https://link.aps.org/doi/10.1103/PhysRevB.92.140409>
- [30] J. Song, H. Dixit, B. Behin-Aein, C. H. Kim, W. Taylor, Impact of Process Variability on Write Error Rate and Read Disturbance in STT-MRAM Devices, *IEEE Transactions on Magnetism* 56 (2020) 1–11. doi:10.1109/TMAG.2020.3028045.  
URL <https://ieeexplore.ieee.org/document/9210520/>
- [31] H. Arai, T. Hirofuchi, H. Imamura, Probability Distribution of the Write-Error Rate of Voltage-Controlled Magnetoresistive Random-Access Memories, *Physical Review Applied* 16 (2021) 064068. doi:10.1103/PhysRevApplied.16.064068.  
URL <https://link.aps.org/doi/10.1103/PhysRevApplied.16.064068>
- [32] T. Maruyama, Y. Shiota, T. Nozaki, K. Ohta, N. Toda, M. Mizuguchi, A. A. Tulapurkar, T. Shinjo, M. Shiraishi, S. Mizukami, Y. Ando, Y. Suzuki, Large voltage-induced magnetic anisotropy change in a few atomic layers of iron, *Nature Nanotechnology* 4 (2009) 158–161. doi:10.1038/nnano.2008.406.  
URL <http://www.nature.com/articles/nnano.2008.406>
- [33] Y. Shiota, T. Nozaki, F. Bonell, S. Murakami, T. Shinjo, Y. Suzuki, Induction of coherent magnetization switching in a few atomic layers of FeCo using voltage pulses, *Nature Materials* 11 (2012) 39–43. doi:10.1038/nmat3172.  
URL <https://www.nature.com/articles/nmat3172>
- [34] S. Kanai, F. Matsukura, H. Ohno, Electric-field-induced magnetization switching in CoFeB/MgO magnetic tunnel junctions with high junction resistance, *Applied Physics Letters* 108 (2016) 192406. doi:10.1063/1.4948763.  
URL <http://aip.scitation.org/doi/10.1063/1.4948763>
- [35] C. Grezes, F. Ebrahimi, J. G. Alzate, X. Cai, J. A. Katine, J. Langer, B. Ocker, P. K. Amiri, K. L. Wang, Ultra-low switching energy and scaling in electric-field-controlled nanoscale magnetic tunnel junctions with high resistance-area product, *Applied Physics Letters* 108 (2016) 012403. doi:10.1063/1.4939446.  
URL <http://aip.scitation.org/doi/10.1063/1.4939446>
- [36] T. Nozaki, T. Yamamoto, S. Miwa, M. Tsujikawa, M. Shirai, S. Yuasa, Y. Suzuki, Recent Progress in the Voltage-Controlled Magnetic Anisotropy Effect and the Challenges Faced in Developing Voltage-Torque MRAM, *Micromachines* 10 (2019) 327. doi:10.3390/mi10050327.  
URL <https://www.mdpi.com/2072-666X/10/5/327>
- [37] W. F. Brown, Thermal Fluctuations of a Single-Domain Particle, *Physical Review* 130 (1963) 1677–1686. doi:10.1103/PhysRev.130.1677.  
URL <https://link.aps.org/doi/10.1103/PhysRev.130.1677>
- [38] H. B. Callen, T. A. Welton, Irreversibility and Generalized Noise, *Physical Review* 83 (1951) 34–40. doi:10.1103/PhysRev.83.34.  
URL <https://link.aps.org/doi/10.1103/PhysRev.83.34>
- [39] H. B. Callen, R. F. Greene, On a Theorem of Irreversible Thermodynamics, *Physical Review* 86 (1952) 702–710. doi:10.1103/PhysRev.86.702.  
URL <https://link.aps.org/doi/10.1103/PhysRev.86.702>



- [40] H. B. Callen, M. L. Barasch, J. L. Jackson, Statistical Mechanics of Irreversibility, *Physical Review* 88 (1952) 1382–1386.  
doi:10.1103/PhysRev.88.1382.  
URL <https://link.aps.org/doi/10.1103/PhysRev.88.1382>
- [41] M. D. Stiles, J. Miltat, Spin-transfer torque and dynamics, in: *Topics in Applied Physics*, Vol. 101, Springer Berlin Heidelberg, 2006, pp. 225–308. doi:10.1007/10938171\_7.  
URL [https://link.springer.com/chapter/10.1007/10938171\\_7](https://link.springer.com/chapter/10.1007/10938171_7)
- [42] J. Sun, Current-driven magnetic switching in manganite trilayer junctions, *Journal of Magnetism and Magnetic Materials* 202 (1999) 157–162.  
doi:10.1016/S0304-8853(99)00289-9.  
URL <https://linkinghub.elsevier.com/retrieve/pii/S0304885399002899>
- [43] J. Z. Sun, Spin-current interaction with a monodomain magnetic body: A model study, *Physical Review B* 62 (2000) 570–578.  
doi:10.1103/PhysRevB.62.570.  
URL <https://link.aps.org/doi/10.1103/PhysRevB.62.570>
- [44] K. J. Lee, O. Redon, B. Dieny, Analytical investigation of spin-transfer dynamics using a perpendicular-to-plane polarizer, *Applied Physics Letters* 86 (2005) 022505. doi:10.1063/1.1852081.  
URL <http://aip.scitation.org/doi/10.1063/1.1852081>
- [45] D. Bedau, H. Liu, J.-J. Bouzaglou, A. D. Kent, J. Z. Sun, J. A. Katine, E. E. Fullerton, S. Mangin, Ultrafast spin-transfer switching in spin valve nanopillars with perpendicular anisotropy, *Applied Physics Letters* 96 (2010) 022514. doi:10.1063/1.3284515.  
URL <http://aip.scitation.org/doi/10.1063/1.3284515>
- [46] D. Bedau, H. Liu, J. Z. Sun, J. A. Katine, E. E. Fullerton, S. Mangin, A. D. Kent, Spin-transfer pulse switching: From the dynamic to the thermally activated regime, *Applied Physics Letters* 97 (2010) 262502. doi:10.1063/1.3532960.  
URL <http://aip.scitation.org/doi/10.1063/1.3532960>
- [47] R. V. Hogg, E. A. Tanis, D. L. Zimmerman, *Probability and Statistical Inference*, 9th edition, Pearson Education, Boston, 2015.